electronics

Article

All-Optical Three-Input "AND" Gate Dependent on a Differential Modulation Architecture

Hassan Termos [1,*] and Ali Mansour [2]

[1] ICFO—The Institute of Photonic Sciences, 08860 Castelldefels, Barcelona, Spain
[2] Lab-STICC, CNRS UMR 6285, ENSTA Bretagne, 2 Rue François Verny, CEDEX 09, 29806 Brest, France
* Correspondence: hassan.termos@icfo.eu

Abstract: This gazette focuses on simulation and experimental studies for all-optical three-input "AND" gate schemes. The proposed gate exploits the semiconductor optical amplifier Mach-Zehnder Interferometer (SOA-MZI) nonlinearities, particularly the cross-phase modulation (XPM) corollary in addition to the cross-gain modulation (XGM) corollary, which originates from a SOA-MZI differential modulation concept. Further, the system performance is analyzed and examined through actual and simulated results to evaluate the obtained "AND" gate signal. Dependent on the nonlinearity of SOAs, the all-optical "AND" gate can operate with three signals driven by a 2 picoseconds (ps) optical pulse source (OPS). We noticed that our experimental results are perfectly matched to the simulated results. The output "AND" signal is acquired at higher common harmonics up to 200 GHz in the simulation study and the optical "AND", which can vastly be used in optical networking, is evaluated through many parameters, such as error vector magnitude (EVM), extinction ratio (ER), and gain. As a result, the pinnacle bit rate for the 16-QAM (Quadrature Amplitude Modulation) and 256-QAM "AND" signal reaches 100 and 200 Gbit/s, respectively, at the 100 GHz common harmonic frequency.

Keywords: all-optical "AND" gate; quadrature amplitude modulation; semiconductor optical amplifier Mach-Zehnder interferometer

Citation: Termos, H.; Mansour, A. All-Optical Three-Input "AND" Gate Dependent on a Differential Modulation Architecture. *Electronics* **2023**, *12*, 1510. https://doi.org/10.3390/electronics12071510

Received: 19 February 2023
Revised: 15 March 2023
Accepted: 22 March 2023
Published: 23 March 2023

1. Introduction

In optical communication nexuses, efficient propositions to logic capabilities play a major role in comparison to electronic signal processing mainly due to their ability to provide faster responses, i.e., almost real time processing. Various systems have been provided to characterize different fundamental logic functions, such as: "AND", "NAND", "OR", or "XOR" gates in the optical discipline [1–4]. Formerly, many concepts have been put forward to accomplish logic gate operations dependent on many optical functional apparatuses including a semiconductor optical amplifier (SOA), an electro-absorption modulator (EAM), and a SOA-Mach-Zehnder interferometer (SOA-MZI) [5–26].

Logic gate concepts can optically be realized through a single SOA as well as its family contingent on the types of interferometers where the MZI is the famous one. There are other mechanisms of the interferometers including the Michelson interferometer (MI) [27] and the Sagnac interferometer (SI) [28] with lower logic gate quality in comparison with the MZI. SOAs have petite dimensions where they can be easily integrated into a variety of electro-optical and all-optical systems in order to achieve mixing as well as logic gate processes. The SOAs display scarce power depletion and can be effectively combined with single-mode fibers (SMFs) because of their structure [29]. Moreover, SOAs are currently the most evolved amplifier in signal processing fields due to their significantly rapid advancement. SOAs are considered to be an attractive design to realize all-optical gate functions thanks to their nonlinearity outcomes, particularly the cross-gain modulation (XGM).

In the XGM concept, the SOA carrier density is modulated by a data signal and this leads simultaneously to gain difference in a control signal inserted to the SOA, which is converted at the wavelength of the data signal at the SOA outturn. The SOA relied on XGM nonlinearity has some drawbacks such as chirping, low extinction ratio (ER), and low-frequency band. The recovery time of applied SOAs is essentially considered as limiting specification for any system, the gain dynamics of SOAs have considerably supported many styling concepts of the data modulation in higher bit rate system applications with outstanding ameliorations in principles of wavelength conversion at a data rate up to 320 Gb/s [30–33].

Additionally, the SOA gain recovery time is alleviated by augmenting the optical intensity of the input photons. This problem can be easily solved by incorporating the SOA in the MZI configuration based on cross phase modulation (XPM) impact, which is shifted to intensity modulation. The XPM nonlinearity is unconstrained to frequencies, in that case, the transformation to a higher frequency is effectively achieved through XPM.

In addition, many principles have been demonstrated to successfully consummate all optical logic "AND" gates dependent on nonlinear features of SOAs, especially the XPM refrain along with the XGM one. Thanks to the benefits of lofty nonlinearity and effortlessness of amalgamation, the SOA-MZI is an excellent determination for "AND" gates by all-optical practicability. Moreover, a logic "AND" gate by all-optical processing as well as its potency are experimentally expounded at the 80 Gbit/s "AND" data rate employing a MZI based differential mode [34–36].

To achieve logic gate operations, Virtual Photonic Inc. (VPI) software [37] can be considered an outstanding candidate. The VPI simulator effectively entrenches huge specialization of optical components and the requirements of optical transmission arrangements in one allocated, resilient software setting to support system performance in structure, investigation, and enhancement with the high acceleration of models of the optical transmission systems. Besides, VPI software provides the most potent numerical procedures customized to telecommunication, radio over fiber (RoF), wireless networks, and high-power and ultrafast applications. It also provides excellent feasibility for minimizing efforts in realistic measurements by employing ready-to-use sophisticated implementations and virtualizing real electrical, photonic, and optoelectronic devices by simulations of components in optical and electrical domains.

In this monograph, we proffer an unparalleled blueprint for a three-input logic "AND" gate contingent on a SOA-MZI assembled on the differential modulation approach, and for the first time, using 2 picoseconds (ps) optical pulse sources (OPSs) at distinct repetition rates. In other words, the exploitation of the three optical signals derived from the OPSs in the SOA-MZI differential modulation with the aim of establishing the "AND" gate signal is unprecedentedly presented in the electrical field. Furthermore, the OPS features including the pulse width period of 2 ps and high repetition rates extremity ameliorate the quality performance of the "AND" signal at the SOA-MZI outlet. Decreasing the duration of the pulse width results in augmentation of the signal bandwidth with which it engages. As alteration become swifter in the time field by minimizing the width duration, this translates to a higher spectral occupation and therefore grander bandwidth. Three input signals with 2 ps pulses are injected into the SOA-MZI simultaneously at different ports to arouse the XPM and XGM effects. The electrical spectrum is the key outcome with the purpose of evaluating the "AND" signal that is achieved at the exit of the SOA-MZI. Using optical filters vanishes unwanted frequency components and enhances different harmonic frequencies of the logic "AND" output. Finally, the logic "AND" signal is fulfilled at the SOA-MZI outlet by connecting three input control OPS channels. This unprecedented system is extremely important because of the vital characteristics of the "AND" signal, which adequately appraises through a medley of crucial specifications including error vector magnitude (EVM) values, extinction ratio (ER), bit error rate (BER) numbers, and range of conversion gains (CGs). These characteristics are considerably improved compared with other systems [34–36]. Furthermore, the way to generate the "AND" signal contingent on the differential modulation mode is unparalleled. The gain measurement and ER of the "AND" signal are electrically assessed, and the measurements of the EVM at high bit transfer rates pending 200 Gbit/s are also achieved to evaluate the "AND" gate, which is attained successfully by all-optical arrangements. Our modern, classic, and flexible design can be practiced in a medley of implementations such as radio over fiber (RoF) and wireless communication networks as well as being employed to build further advanced complex logic circuits.

2. Operation "AND" Principle

In our work, the primary assumption to achieve logic gate processes is a configuration called differential modulation where the "AND" gate signal is successfully attained at the SOA-MZI exit. This principle is proficiently employed to identify a transmission window [38,39] of the logic gate signal contingent on the differential modulation mechanism. In this principle, a pulsed signal is introduced at both parts of the interferometer through SOA-MZI middle port. In contrast, two other pulsed signals with different parameters are injected in the uppermost and bottom arms of the SOA-MZI structure. At the SOAs outturn, the high gain and phase are effectively realized after modulating their carrier densities as well as their refractive indexes. At the SOA-MZI output, the differential transmission window of the "AND" signal is obtained after combining the optical signals generated from both SOAs by means of an optical coupler (OC). The "AND" transmission window follows the cosine of phase variation and SOA gains as a consequence of the XPM and XGM effects. As a result, two pulsed control signals are modulated by another pulsed signal and the employed SOA-MZI in this concept acts as a modulator. The SOA-MZI design is applied in the differential modulation procedure where three pulsed control signals affect the logic gate state. In that case, in this duration of the transmission window, we can attain the "AND" signal, which is quite fast due to the gain recovery time of both SOAs. The differential modulation mode plays a vital role to ameliorate the efficiency of an optical "AND" gate transmission system because all pulsed signals are consummated at one of the wavelengths of the control pulsed signal. This greatly amplifies the power and reduces the noise of the logic "AND" gate signal at the SOA-MZI output.

The "AND" gate field can optically come into possession of a SOA-MZI as demoed in Figure 1. This efficient SOA-MZI is employed as an optical ON/OFF device or a sampling mixer and can also be utilized as a logic gate. Moreover, the SOAs in both arms are expected to be identical, therefore, to realize a Boolean product $Q = A * B * C$ that is the multiplication of the three input signals. The second one is the incoming signal B at a frequency of $f_2 = 10$ GHz that enters the middle port (MP), cleaves evenly into two portions at the bottommost and uppermost arms, and has harmonics at frequencies $H_n = nf_2$. Besides, the first input signal A at $f_1 = 5$ GHz is introduced into the upper port (UP) having harmonics at $H_m = mf_1$. Lastly, the input signal C at $f_3 = 20$ GHz is inserted into the lower port (LP) having harmonics at $H_p = pf_3$ where the harmonic ranks n, m, and p are strictly positive integers. A, B, and C have conceptual electrical spectrums as showcased in Figure 1.

At the SOA-MZI output, distinctive band pass filters are optically implemented intending to only achieve the "AND" gate function because, at the same time, the mixing function between the three input signals can be obtained as well at the output port on the basis of the XPM and XGM repercussions in the SOAs. Thus, the requested signal Q at the output porthole is actually the by-product of a Boolean product of three incoming signals $A * B * C$. Since the three inward signals have common harmonics ($H_4^A = H_2^B = H_1^C = 20$ GHz and $H_8^A = H_4^B = H_2^C = 40$ GHz), the output "AND" signal (Q signal) will have harmonics H_1^Q and H_2^Q as well as different amplitudes resulting from the power product of each input signal $P_{H_1^Q} = P_{H_4^A} * P_{H_2^B} * P_{H_1^C}$ at $H_1^Q = H_4^A * H_2^B * H_1^C = 20$ GHz and $P_{H_2^Q} = P_{H_8^A} * P_{H_4^B} * P_{H_2^C}$ at $H_2^Q = H_8^A * H_4^B * H_2^C$ at 40 GHz.

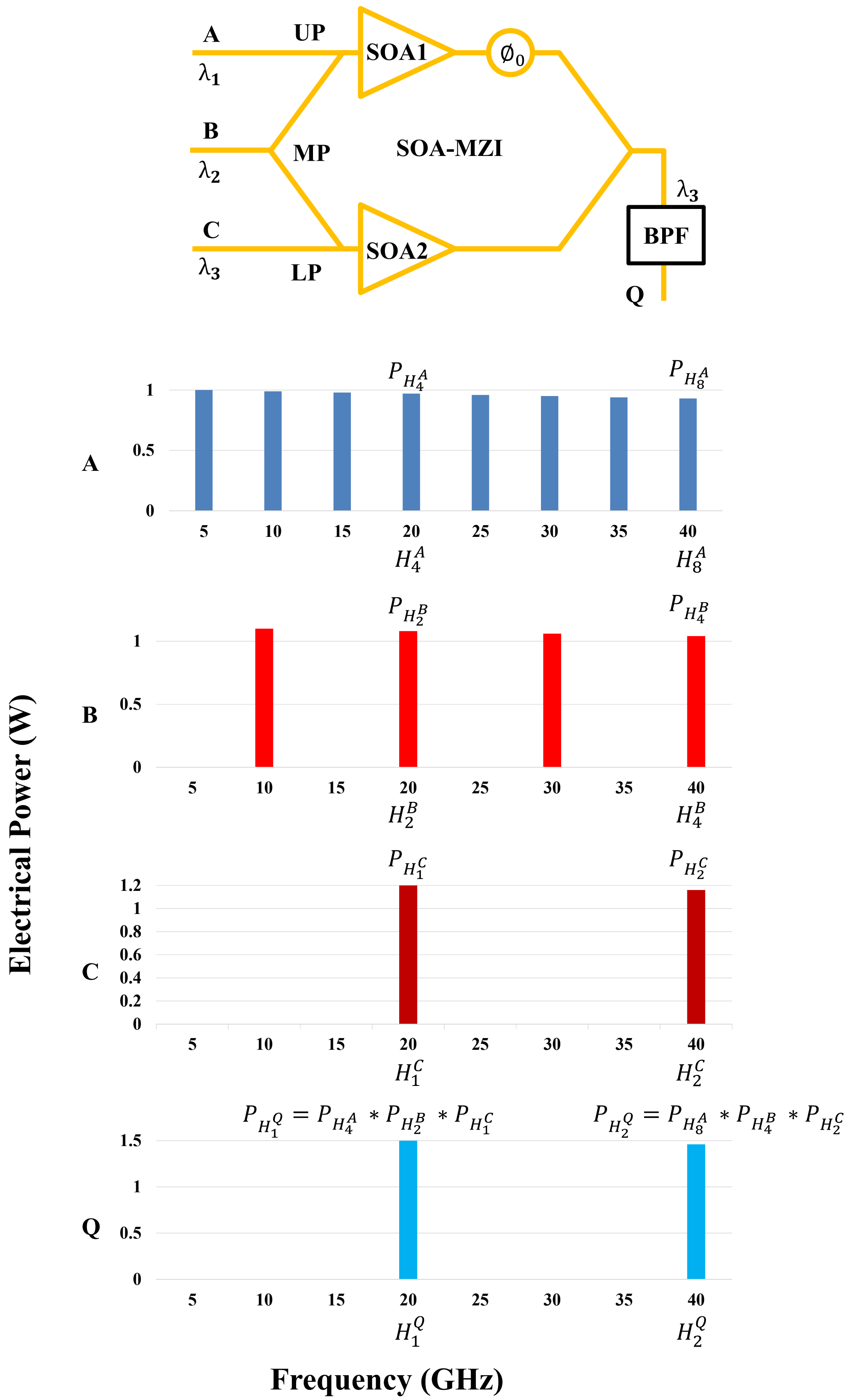

Figure 1. Silhouette of the principle of three-input "AND" gate based on the sampling SOA-MZI using its differential modulation architecture. SOA: Semiconductor Optical Amplifier, BPF: Band pass Filter, UP: Upper port, MP: Middle Port, SOA-Mach-Zehnder Interferometer (SOA-MZI), LP: Lower Port, A, B, and C are input signals, Q is the output "AND" signal, and $\varnothing_0$ is the phase shifter.

Furthermore, the "AND" signal is effectuated at the SOA-MZI outturn thanks to the SOA-MZI nonlinearities including XGM and XPM ramifications. Besides, the applied filter is optically tuned at the third input signal wavelength λ_3 and the other two incoming signals are metamorphosed at λ_3 at the outturn of the SOA-MZI because of the XGM impact.

The physical existence of the wave A along with the signal C affects the phase of the wave B at the topmost and lower parts owing to the XPM effect in SOAs. As a consequence, the high increment of the OPS repetition rate results in effectively modulating the SOAs carrier density with a minuscule duration of OPS pulses that leads to reduced alteration of harmonics amplitude with the harmonic ranks n, m, and p. Consequently, the "AND" signal is considerably validated its attributes, which are upgraded at the SOA-MZI outlet.

When the incoming wave A is ON in the upstairs arm and the input signal C is also ON in the downstairs arm, a phase shift stimulated on the wave B at both arms occurs. As a result, the signals A and C, which are ON, generate a phase shift on the signal B, which moves normally across the pair arms and intervenes at the outturn. Thus, if A, B, and C are ON, the multiplied signal output is ON while if one of them, A, B, or C, is OFF, there will be no phase shift, and hence the product output that corresponds to the "AND" signal is OFF and consequently the logic gate function "AND" is effectively achieved. Notably, ON represents True or 1 and OFF represents false or 0. On the other hand, it is crucial to mention that if one of the three signals is ON, this signal is remarkably magnified at the SOA-MZI outturn, however, it never corresponds to the "AND" signal. Furthermore, if two of the three signals are ON, then these waves are mixed at the exit of the SOA-MZI and consequently the mixed signal also never corresponds to the "AND" signal. Correspondingly, the "AND" signal is only realized when the three input signals are ON.

3. Experimental Characterizations of the OPS Developed on a SOA-MZI Stratifying Differential Modulation Approach

The architecture of a SOA-MZI concocted by an old company known as the center for integrated photonics (CIP) in electrical and electronic sciences [37,39] is propounded in Figure 2. The employed interferometer has two sectors where one SOA is put down in each sector of the MZI. The phase shifter ($\varnothing_0$) that corresponds to a detached thermo-optic one and is puzzled out in the celestial sector assists to tool up signal phase amelioration at the outturn topmost and lower parts of the interferometer. The $\varnothing_0$ regulation is employed in order to attain the lowest optical average power at the SOA-MZI outturn when there is a nonexistent control signal at the uppermost and undermost gates of the SOA-MZI input. As a result, its function is to identify the best operating parameters of the SOA-MZI, which is applied in a variety of functions such as the logic gate operation. Additionally, the experimental setup exploits the applied SOA-MZI in its differential modulation architecture.

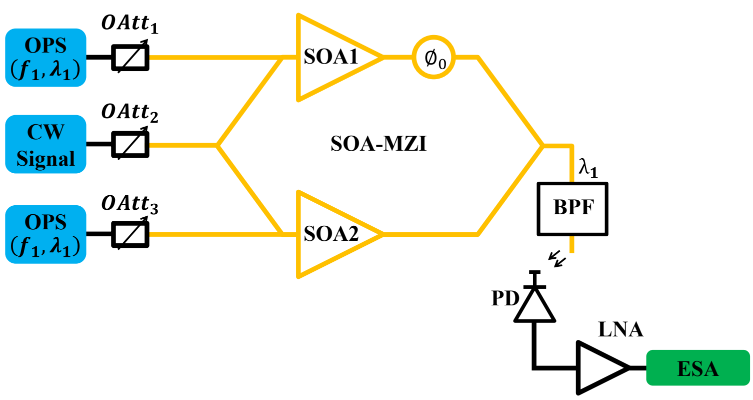

Figure 2. Experimental Setup for OPS response at the SOA-MZI output. OPS: Optical Pulse Source, $OAtt$: Optical Attenuator, ESA: Electrical Spectrum Analyzer, CW: Continuous Wave, PD: Photodiode, and LNA: Low Noise Amplifier.

The applied optical pulse source (OPS) has the same attributes in this setup and is fabricated by Pritel Inc. [37–44]. The OPS has features of 2 ps width optical pulses, which can be obtained at the optical frequency of $\lambda_1 = 1550$ nm and the repetition rate of $f_1 = 5$ GHz. The OPS harmonics are carefully studied on an ESA where their electrical power minimizes with the harmonic frequency as exhibited in Figure 3. There are various factors including the OPS pulse shape, the OPS duty cycle, the frequency scope of the applied photodiode (PD), and the electrical gain of the low noise amplifier (LNA), which mainly influence the OPS harmonics. The harmonic power levels have different values where the power disparity of the control OPS signal between the fifth harmonic at $H_5 = 5f_1 = 25$ GHz and the first one at $H_1 = f_1 = 5$ GHz is roughly 10 dB. The power at $f_1 = 5$ GHz is the higher one owing to its frequency, which is near the cut-off frequency of the used SOA-MZI [37].

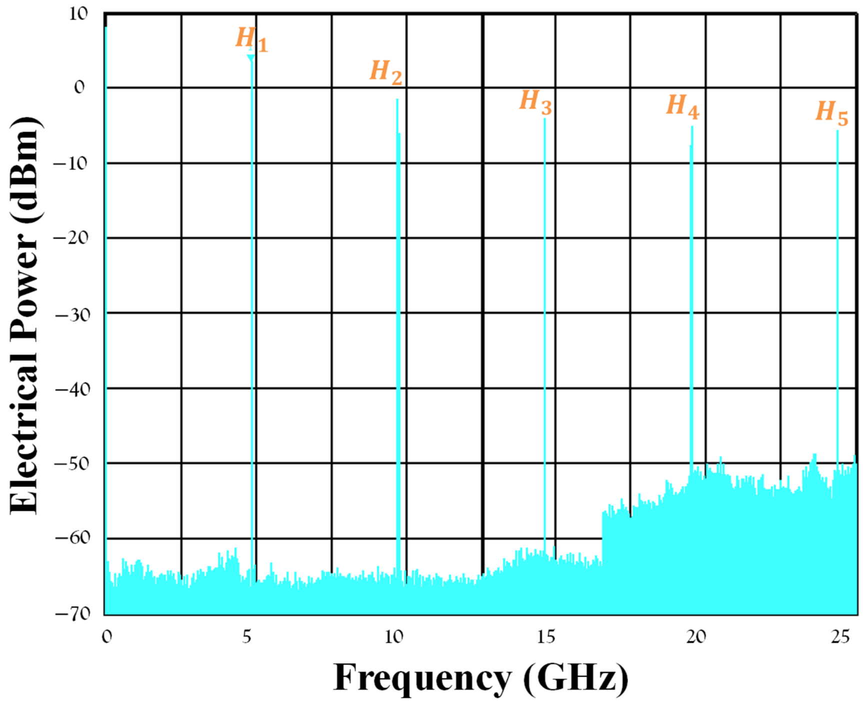

Figure 3. The OPS harmonics obtained through an ESA at a 5 GHz repetition rate at the incoming port of the employed SOA-MZI.

The SOAs' physical elements in the interferometer are identical, whereas the most crucial SOA ones are propounded in Table 1. The main characteristics with and without modulations are already highlighted in [39,45] for the purpose of pinpointing the excellent operating point applied to the "AND" gate approach. The dynamic feature of the employed SOA-MZI device is contingent on the differential carrier lifetime (τ_d) in addition to the stimulated carrier recombination time (τ_s). In accordance with the applicable SOAs, the congruous effective carrier lifetime (τ_e) exclusively enlarges from tens to hundred ps, as demonstrated in Equation (1) [46]. That is why the SOAs have to be biased at the elevated bias current of 400 mA. In order to maintain an outstanding "AND" effectiveness of all-optical arrangements, the requested time of both SOA's gain and phase requires to regain speedily. In addition, this recovery time places reliance on the input optical wavelength [47,48], which must be proximate enough to fulfill rapid recovery. In spite of its rapid runtime, the congruous SOAs in the interferometer precisely contemplate a manifold of accelerated XPM and XGM nonlinear effects and extreme dynamics. Hence, the obvious investigation of the coplanar operating point of the "AND" transmission system will advantageously identify the leverage of SOAs parameters on the quality of M-QAM "AND" data transmission.

$$\tau_e = \frac{\tau_d \tau_s}{\tau_d + \tau_s} \tag{1}$$

Table 1. The amounts of the SOAs element employed in the empirical and simulated setups.

Elements	Amounts
Linewidth enhancement factor	4
Differential Carrier Lifetime	27 ps
Effective Carrier Lifetime	72 ps
SOA Saturation Power	15 dBm
SOA1 Gain	27.5 dB
SOA2 Gain	28.5 dB
SOAs Current	400 mA

The OPS is injected into the incoming port of the SOA-MZI and consequently crosses the SOAs in each sector at the same repetition rates and wavelengths. Hence, the carrier densities in the SOA1 and SOA2 active regions transition as well as their refractive indexes are mutated. This fundamentally effectuates the cross phase modulation (XPM) consequence on the continuous wave (CW) data wave in every sector. Therefore, the interference at the exit of the employed SOA-MZI develops in a constructive way as propounded in Figure 4, which represents the harmonics power of the amplified OPS signal, and culminates in an optical mean power (P_{out}) at the SOA-MZI outbound, which is given by Equation (2). This inequality shows the variation of the SOA1 and SOA2 gains and phases, because of XPM and XGM nonlinearities in every sector [45].

$$P_{out} = \frac{P_C}{4}\left(G_{out1}(t) + G_{out2}(t) - 2\sqrt{G_{out1}(t)G_{out2}(t)}\cos(\varnothing_o + \phi_{out1}(t) - \phi_{out2}(t))\right) \quad (2)$$

where P_C embodies the average power of the incoming field C anterior to SOA2, $G_{out1}(t)$ is the time-dependent gain of SOA1, $G_{out2}(t)$ is the time-dependent gain of SOA2, $\phi_{out1}(t)$ stands for the phase shift in SOA1, and $\phi_{out2}(t)$ is the phase shift in SOA2.

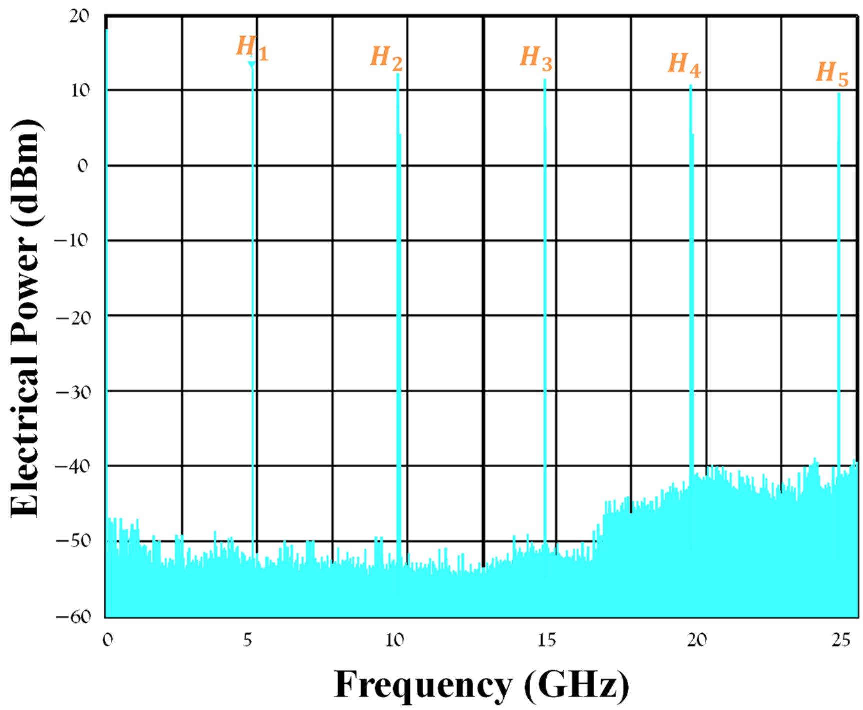

Figure 4. The characteristics of the OPS signal after optical amplification at the SOA-MZI outturn.

A CW optical power of −10 dBm for the data signal at the wavelength of 1545 nm is injected at the common incoming port of the SOA-MZI where the BPF (Band Pass Filter) wavelength at the SOA-MZI outbound is tuned at $\lambda_1 = 1550$ corresponding to the OPS wavelength. The output wave, corresponding to the OPS signal after optical amplification, is morphed into an electrical one by applying a photodiode (PD) and then augmented by employing a low noise amplifier (LNA) that has 33 dB gain before being displayed on the electrical apparatus known as a spectrum analyzer (ESA).

Figure 4 exhibits the enhancement of the OPS signal at the exit of the SOA-MZI. The whole OPS harmonics are extremely augmented compared to its harmonics at the SOA-MZI incoming. Table 2 below presents the conversion gain (CG) at $H_n = nf_1$, which is demonstrated as the distinction in electrical powers between the inbound OPS harmonics at the inlet of the SOA-MZI and the harmonics of the amplified OPS signal at the exit of the SOA-MZI.

Table 2. The conversion gain for the amplified OPS field at the exit of the SOA-MZI at nf_1.

Harmonic Frequencies at nf_1 (GHz)	Input Power Harmonics at nf_1 (dBm)	Output Power of Harmonic at nf_1 (dBm)	Gain (dB)
$f_1 = 5$	5	15	10
$2f_1 = 10$	−2	13	15
$3f_1 = 15$	−4	11.5	15.5
$4f_1 = 20$	−5	10.5	15.5
$5f_1 = 25$	−5.5	9.5	15

Figure 2 is only used to achieve amplification of the OPS signal at the SOA-MZI output. In this measurement, we have determined at the SOA-MZI output that we can obtain only harmonics of the OPS signal that may correspond to the "AND" signal if we have developed the principle presented in Figure 2. Furthermore, the performance attributes of the applied optical amplification system dependent on the differential modulation concept using an efficient SOA-MZI through conversion gain (CG), error vector magnitude (EVM), extinction ratio (ER), and bit error rate (BER) will be grossly improved at the system output. This type of system can be a benefit in a diversity of implementations including microwave and radar networking, wireless complexes, and radio over fiber. On the other hand, the transformation of the CW signal to one that alters with time achieves many significant functions at the SOA-MZI output, specifically the "AND" logic gate.

4. Experimental and Simulated "AND" Gains

Hereinafter, we propose three-input "AND" logic contingent on an all-optical single SOA-MZI harnessing widely known technique under the name of the differential modulation architecture. Additionally, optical filtering plays a vital role to help realize the "AND" signal in our setup. The empirical setup is presented in Figure 5, which is similar to Figure 2. However, the only difference between them is that the CW signal is altered to be an OPS signal and all the OPS signals have various repetition rates and wavelengths in order to substantiate the "AND" gate concept. In our experimental studies, we utilized the SOA-MZI based on CIP technologies where the simulated SOA-MZI [45,49] used in the VPI software [37] has related characteristics to the actual SOA-MZI [37].

In our study, experimental and simulation setups have the same operating points in which the SOAs are biased at 400 mA to enhance the XPM effect. Three optical input signals are introduced to evoke the nonlinear SOA-MZI and cause the XPM impact. The three signals, which are synchronized and driven by the OPSs, having the same structure and characteristics, in turn, have the same pulse width duration of 2 ps, different repetition rates, and different wavelengths. The first signal, A, is entered at the SOA-MZI upper port (UP) at the optical frequency of $\lambda_1 = 1550$ nm at the frequency $f_1 = 5$ GHz, the second signal, B, is interpolated at the SOA-MZI middle port (MP) at $\lambda_2 = 1551$ nm at $f_2 = 10$ GHz, and the final one, C, is introduced at the SOA-MZI lower port (LP) at $\lambda_3 = 1552$ nm at $f_3 = 20$ GHz. As a consequence, we conjecture that the inbound signals possess an identical peak power of -5 dBm.

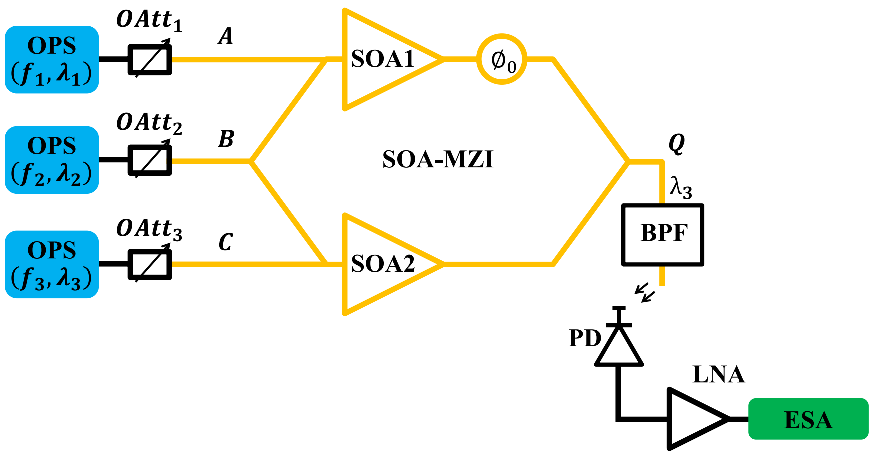

Figure 5. All–optical "AND" gate setup dependent on the SOA-MZI using a differential modulation architecture for the experimental and simulation studies.

The subsequent band-pass filter (BPF), which is optically regulated at the OPS wavelength of the third signal $\lambda_3 = 1552$ nm, is employed at the SOA-MZI output to extract different sideband spectrums. The aim is to keep the common harmonics, especially at 20 and 40 GHz, between the three input signals at the exit of the SOA-MZI. The BPF can extremely be applied to single out the common harmonics while dismissing all other harmonics and replicas related to frequency mixing. As a result, the BPF is employed to only maintain the harmonics of the "AND" signal. It is worth noting that the first and second signals will be converted at the wavelength of λ_3 at the SOA-MZI outturn according to the XGM impact. Thus, at the BPF outturn, the filtered optical signal is converted to the electrical one by a PD and then considerably intensified by a LNA. Lastly, the outbound "AND" signal is efficiently achieved at the output of the SOA-MZI originating from the multiplication of three inbound OPS signals in the electrical field through a spectrum analyzer.

In Figure 6, the effective consequences for the proposed "AND" gate signal in the realistic and simulated investigations at the exit of the SOA-MZI are well validated in the electrical discipline where the electrical power is matched up against the two common frequencies of 20 and 40 GHz. The obtained results corroborate the performance of the novel scheme of the "AND" gate when the three input signals are at 20 and 40 GHz, the "AND" signal, which beneficially conforms to the multiplicity of the three inbound OPS signals, has also these common harmonic frequencies. The extinction ratio (ER) feature, which is fundamentally expounded as the variation between the larger and lower numbers of electrical powers of the outbound "AND" signal, is measured at the SOA-MZI outturn. At 20 GHz, the ER of 56 dB is achieved through simulations; while, it shows 54 dB for the real experimentation. In both cases, the ER diminishes by 6 dB at 40 GHz. It is important to mention that a mixing function can be attained at the exit of the SOA-MZI between the inbound signals. Onward, the mixed signals are unconditionally removed by the OBPF to validate the "AND" gate process.

In the simulation study, we discerned that the results are attainable and that we could achieve the "AND" operation at the output place of the employed SOA-MZI at the higher common harmonic frequencies that recently reached 200 GHz as presented in Figure 7. Noting that the whopper frequency range of the novel "AND" signal system is 200 GHz, which is the highest range realized, for the first time, for the "AND" gate signal. For instance, the harmonic H_{10}^{Q} of the output "AND" signal represents the multiplication of harmonics $H_{10}^{C} = 10f_3$ related to the third input OPS signal, C, $H_{20}^{B} = 20f_2$ related to the second input OPS signal, B, and $H_{40}^{A} = 40f_1$ related to the first input OPS signal, A, that is, $H_{10}^{Q} = H_{10}^{C} * H_{20}^{B} * H_{40}^{A}$.

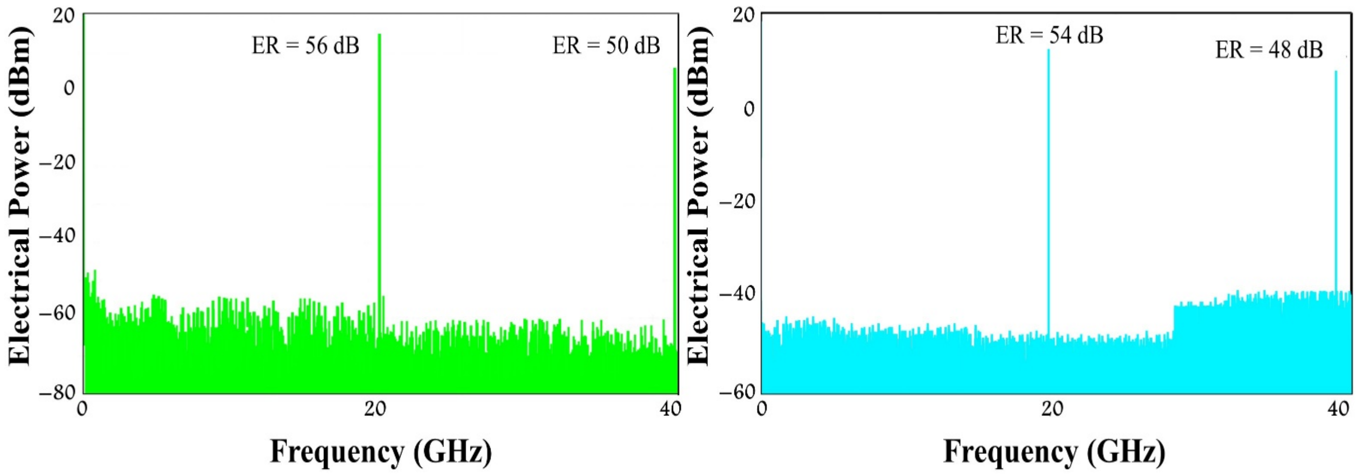

Figure 6. Simulation (at **left**) and experimental (at **right**) results for the "AND" gate signal contingent on the SOA-MZI differential modulation concept. ER: Extinction ratio.

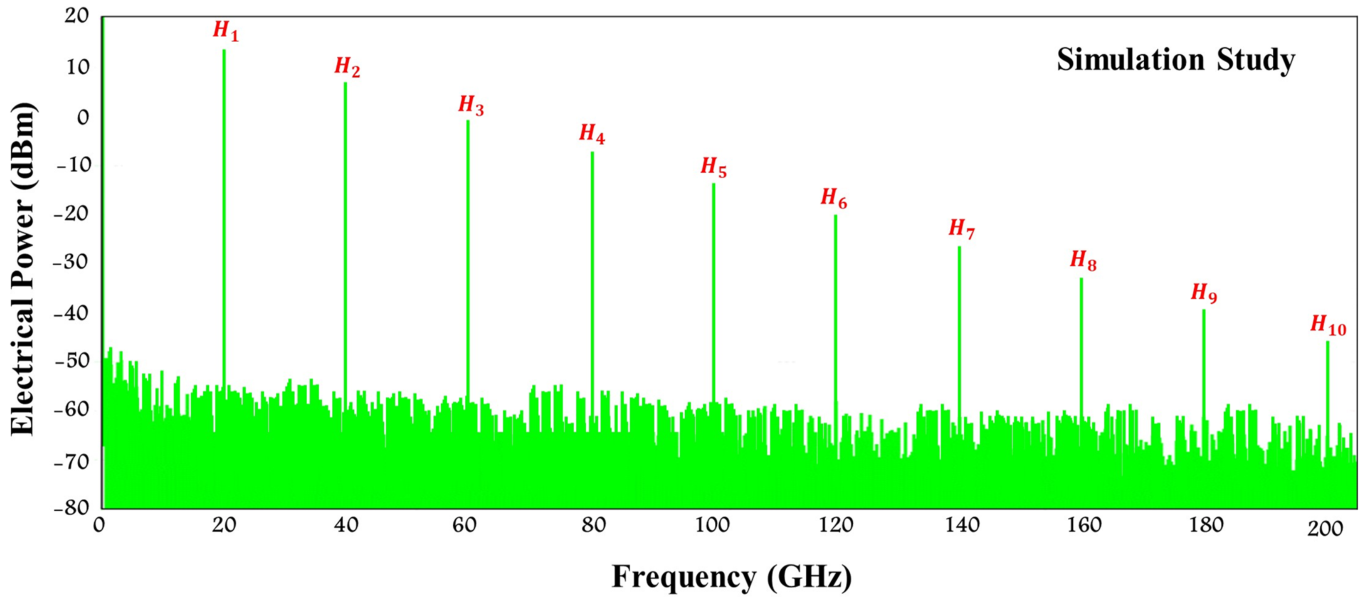

Figure 7. Electrical spectrum results successfully attained by the VPI simulator for the "AND" gate mechanism using the differential modulation concept.

The "AND" signal at the outturn of the applied SOA-MZI is a consequence of two optical "AND" signals generated by both SOAs with the aim of improving the quality performance of the "AND" signal thanks to the extremely lofty gain of the SOAs contingent on the XPM and XGM nonlinearities. The electrical power of harmonics decreases with the common frequency at the SOA-MZI output. The investigation of the differential modulation concept upgrades the power of the "AND" signal, especially at the high common frequency. In that case, we can obtain the "AND" signal at the common frequency up to 200 GHz. During, the experimental study, we could achieve the "AND" signal at 40 GHz due to the limitation of the frequency scope of the employed ESA. As a result, it is impossible to obtain the "AND" signal at any harmonic frequency because of the dynamic behavior of the used SOA-MZI [38,39]. After 200 GHz, the electrical power considerably reduces with the common frequency, which frequently deteriorates the efficiency of the "AND" telecommunications system.

The below tables considerably validate the principle of the "AND" gate process and effectively assess its performance. The electrical conversion gain is principally demonstrated as the difference between the outbound "AND" signal at 20 and 40 GHz and the three inbound OPS signals at the same frequencies and is exhibited in Tables 3 and 4 at 20 and 40 GHz, successively for the empirical work. Furthermore, the outbound harmonic power is 13 dBm at 20 GHz and 7 dBm at 40 GHz. Otherwise, the OPS power of the input signals at 20 and 40 GHz aggrandizes with the augmentation of the amounts of the repetition rate from 5 to 20 GHz. Furthermore, the degradation of the harmonic power at 40 GHz is up to 6 dB in comparison with the one at 20 GHz.

Table 3. The gain for the realistic "AND" signal practicability at the lower common harmonic frequency of 20 GHz.

Repetition Rate (GHz)	Input Harmonic Power at 20 GHz	Output Harmonic Power at 20 GHz	Gain (dB)
5	−5	13	18
10	3.5	13	9.5
20	6.5	13	6.5

Table 4. The gain for the realistic "AND" signal practicability at the higher common harmonic frequency 40 GHz.

Repetition Rate (GHz)	Input Harmonic Power at 40 GHz	Output Harmonic Power at 40 GHz	Gain (dB)
5	−10	7	17
10	−1.5	7	8.5
20	1.5	7	5.5

At the way out of the applied SOA-MZI gate, the measured gain at 20 GHz declines from 18 to 6.5 dB with the repetition rate. Additionally, we observe similar behavior for the gain at 40 GHz compared to the one at 20 GHz due to the outbound "AND" signal, showing a perfect multiplication of three signals at two different harmonic powers of two various common harmonics frequencies, in addition to the SOA-MZI amplification. It is important to mention that the reduction in the "AND" signal intensity of the common harmonics is a consequence of the dynamic SOA-MZI characterizations.

The gain at the egression of the SOA-MZI port is assessed further for the simulation work over the complete ambit of common harmonic frequencies that reach 200 GHz, as presented in Figure 8. Therefore, the gain comparison among the simulated and experimental outcomes shows close results. However, there is a decrease of 2 dB for the actual measurements. This regression is due to the real "AND" signal that faces more unexpected noises including mainly thermal noise, PD shot noise, and SOAs amplified spontaneous emission (ASE) noise.

Figure 8 additionally portrays that the experimental gain results at the common harmonic frequencies of 60, 80, and 100 GHz, cannot be presented in Figure 6 because of the limited bandwidth of 40 GHz with respect to the used ESA. Hence, the realistic "AND" signal at 60, 80, and 100 GHz is shifted to 0.5 GHz by using an electric mixer. The simulated gain decreases when the common frequency increases from 20 to 100 GHz as well as the actual gain; while, it increases when the common frequency augments from 100 to 200 GHz. This behavior is due to of the differential modulation architecture that considerably augments the outbound "AND" signal intensity. The disparity between the harmonics power H_{10} and H_1 of the outbound "AND" signal is 61 dB as noted in Figure 7. It is extremely important to point out that the OPS signal power at the entry of the SOA-MZI gate deteriorates deeply with the harmonic frequency.

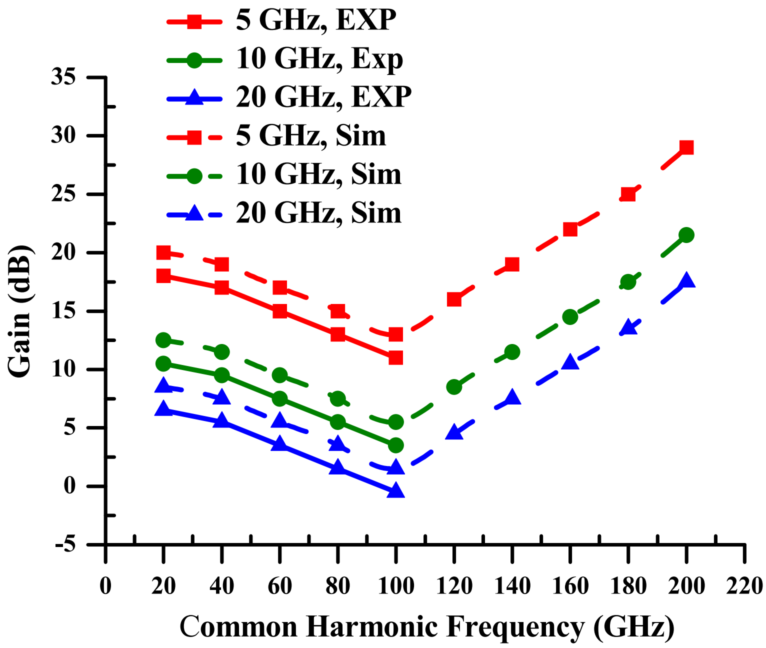

Figure 8. The experimental and simulated conversion gains for the outbound "AND" signal.

The XPM and XPM nonlinearities in the used SOA-MZI lead to achieving an "AND" signal at the SOA-MZI outlet, which has high efficiency at low input average powers. In addition, the "AND" signal is ameliorated by augmenting the active region distance and the bias current of each SOA. It is vital to mention that the real work has unavailability to control the length of the active region because it is a physical parameter inside the apparatus while it is possible in VPI simulations.

5. Experimental and Simulated Results of M-QAM "AND" Signal

In order to generate the M-QAM (quadrature amplitude modulation) data modulation, we need a particular type of generator that is known as an arbitrary wave generator (AWG). On the other hand, at the SOA-MZI output, the "AND "signal has to be demodulated for the purpose of evaluating the quality performance of the "AND" gate system. Because of that, a digital sampling oscilloscope (DSO) in combination with a software called vector signal analyzer (VSA) is applied at the SOA-MZI outlet. As a result, Figure 5 is developed to acquire the M-QAM "AND" signal as demonstrated in Figure 9.

The experimental and simulation setups contingent on the SOA-MZI applying complex modulation formats are covered in Figure 9 for the differential modulation approach. M-QAM data are derived from an AWG for the experimental work or the generation and detection design for the simulation one at a frequency $f_3 = 20$ GHz. In this work, 4-QAM, which is also known as QPSK (Quadrature Phase Shift Keying), 16-QAM, and 256-QAM are chosen in order to be examined for the outbound "AND" system. An electrical signal from the AWG modulates an optical carrier carrying 4-QAM, 16-QAM, and 256-QAM at the wavelength of $\lambda_3 = 1552$ nm using an optical MZM where its output is introduced at the lower SOA-MZI gate. Similarly to our experimental and simulation setups, the outbound "AND" output signal is optically filtered by a BPF, and then converted to the electrical field by the PD and magnified by the 33-dB LNA. Thereafter, a DSO for the actual work and the BER_El-M-QAM module for the simulated work are effectively utilized to digitalize and demodulate the outbound M-QAM "AND" signal where M is studied on three values that are equal to 4, 16, and 256.

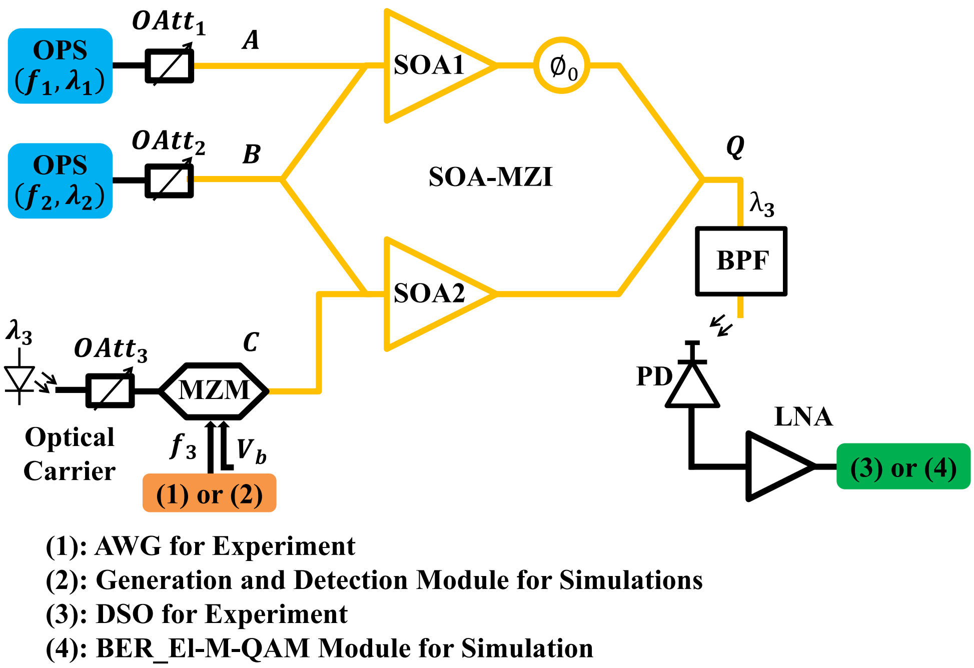

Figure 9. M-QAM "AND" setup contingent on the SOA-MZI employing differential modulation approach. AWG: Arbitrary Waveform Generator, DSO: Digital Sampling Oscilloscope, BER: Bit Error Rate, V_b: Bias Voltage, and MZM: Mach-Zehnder Modulator. The other initialisms are described as in Figure 5.

The quality of the M-QAM "AND" signal dependent on the SOA-MZI differential modulation concept is commonly appraised by comprehending the error vector magnitude (EVM) [50] amounts through VSA software over bit rate specifications. This criterion is generally associated with the bit error rate (BER) calculations, and the agreeable restriction is explicated as a number that imparts a tantamount BER of 3.8×10^{-3}, which corresponds to 35% EVM after stratifying the modus operandi of the forward error correction (FEC) [51,52]. The 4-, 16-, and 256-QAM constraints are 17.5, 12.5, and 3.5%, respectively, which are applied in a medley of applications [53,54] and they are effectively used in this work.

In Figure 10, for the 16-QAM "AND" signal, the 100 Gbit/s bit rate is exceptionally realized for the common harmonic frequencies ranging from 20 to 100 GHz at the outbound port of the SOA-MZI by utilizing the differential amendment concept. The EVM of the "AND" signal carrying 16-QAM data augments with the common harmonic frequency. It further escalates with the bit rate as well. The investigation of the differential amendment architecture contingent on the applied SOA-MZI ameliorates the obtained outcomes of the entire optical "AND" transmission arrangement. Thus, this architecture leads to demodulating the 16-QAM "AND" signal at the extremely high bit rate that is 100 Gbit/s, for the first time, at the paramount frequency scope of 100 GHz for both studies where the experimental EVM reaches 12.5% at 100 Gbit/s at 100 GHz. Furthermore, there is a perfect conformity between the simulated and experimental studies, and it is worth noting that there is a possibility to demodulate the 16-QAM "AND" signal at the outbound gate of the efficient SOA-MZI at the higher common harmonic frequencies up to 200 GHz in conjunction with high bit rates in the simulation study through the VPI software.

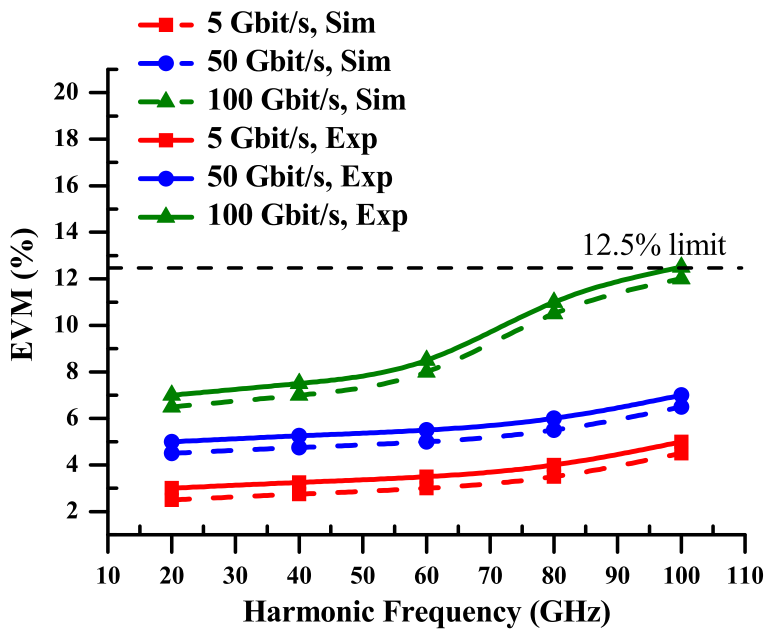

Figure 10. The experimental and simulated EVMs at the SOA-MZI output for the 16-QAM "AND" signal at several bit rates and common harmonics frequencies.

At the SOA-MZI input, the experimental back to back (BtB) amount of the 16-QAM EVMs, which originate at $f_3 = 20$ GHz by an optical MZM, is appraised at the MZM output. It augments from 0.5% at the 5 Gbit/s bit rate to 2.5% at 100 Gbit/s as presented in Figure 11.

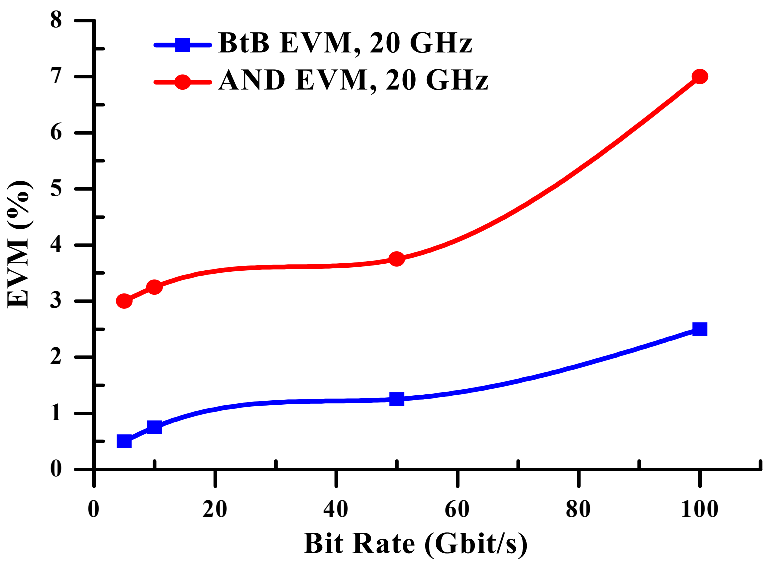

Figure 11. Experimental back to back (BtB) values of the 16-QAM EVMs and the 16-QAM "AND" signal at 20 GHz for a miscellany of bit rates.

This 16-QAM "AND" signal at 20 GHz ranges from 3% at 5 Gbit/s to 7% at 100 Gbit/s at the outbound gate of the used SOA-MZI as also displayed in Figure 10. The rapid increase in numbers of the bit rate results in incrementing the 16-QAM bandwidth (BW). This consequently instigates to enlarge noise power while the aggregate signal power is not amended.

Figure 12 presents the reliance of the BER parameter onto EVM one for the 16-QAM "AND" field at the 100 Gbit/s bit rate for the experimental outcomes. The values of the EVM and BER characters are successfully obtained when the inbound data power is −10 dBm. It is essential to mention that the reduction in the electrical CG of the "AND" signal in Figure 8 causes an increment in the values of the EVM and BER merits. The maximal experimental BER value is 0.00056, which corresponds to a 12.5% EVM value.

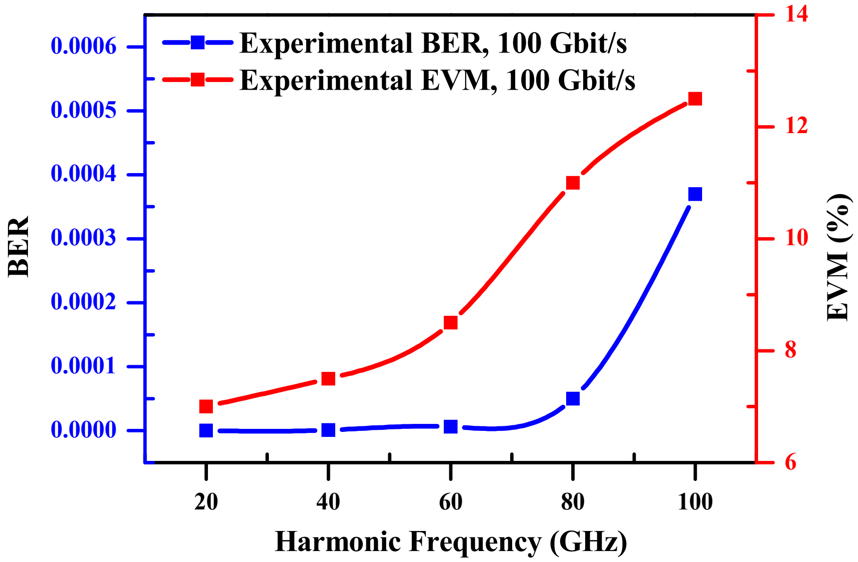

Figure 12. Experimental BER and EVM amounts in opposition to the harmonic frequency for the "AND" signal at 100 Gbit/s in the case of 16-QAM modulation.

A multiplicity of complex M-QAM modulations is applied for the "AND" signal at the exit of the SOA-MZI at the symbol rate of 25 Gbit/s as given in Figure 13 and their EVM values are monitored for the purpose of evaluating the optical system attributes of the "AND" principle contingent on the employed SOA-MZI using the differential modulation schema.

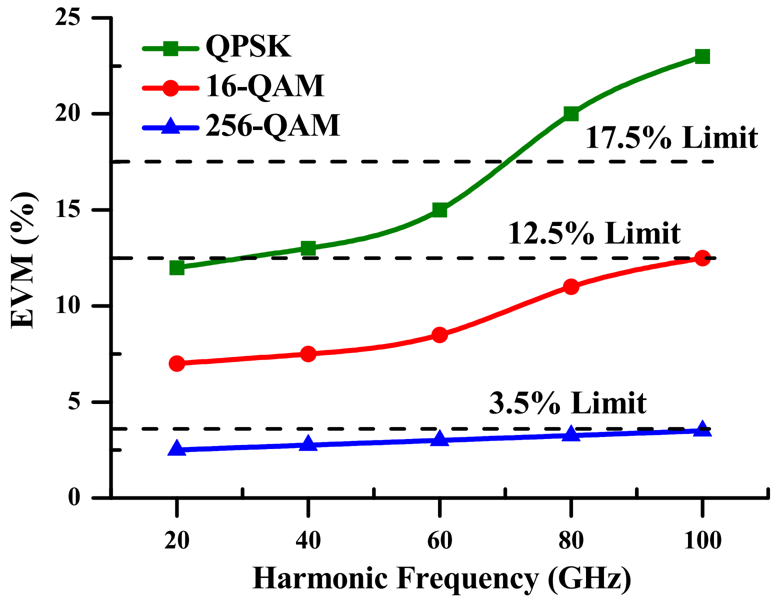

Figure 13. Experimental EVM values versus the harmonic frequency for the "AND" signal at symbol rate of 25 Gbit/s in the case of 4-, 16-, and 256-QAM modulations. QPSK: Quadrature Phase Shift Keying.

The EVM is plotted against harmonic frequencies for 4-, 16-, and 256-QAM modulations in Figure 13 where the maximum bit rates, which is defined as a multiplication between the bits number and the symbol rate, of 4-, 16-, and 256-QAM "AND" signals at the outbound port of the SOA-MZI are 50, 100, and 200 Gbit/s, respectively. Furthermore, the EVM values have been ameliorated by augmenting the whole number of bits of M-QAM modulation [49,55] by virtue of the enlargement in the signal-to-noise (SNR) ratio. Besides, the utmost EVMs are 23, 12.5, and 3.5%, respectively, for 4-, 16-, and 256-QAM at the harmonic frequency of 100 GHz. As a consequence, the EVM values of all 4-, 16-, and 256-QAM "AND" signals have the same behavior, which augments with the decrease of the harmonic frequency.

The constellation diagrams of 4-, 16-, and 256-QAM "AND" signals are portrayed in Figure 14. These diagrams are ones of the many constellation diagrams obtained by the VSA software application. The 4-QAM "AND" signal has a constellation diagram where its EVM value is 12% at the harmonic frequency of 20 GHz at the 50 Gbit/s bit rate seen in Figure 14a. The 16-QAM "AND" signal has two constellation diagrams, the first one has an EVM value of 5.5% at 20 GHz at 50 Gbit/s in presented Figure 14b and the second one has an EVM amount of 3% at 20 GHz at 5 Gbit/s shown in Figure 14c. Lastly, the 256-QAM "AND" signal has a constellation diagram where its EVM amount is 0.5% at 20 GHz at 50 Gbit/s, as propounded in Figure 14d.

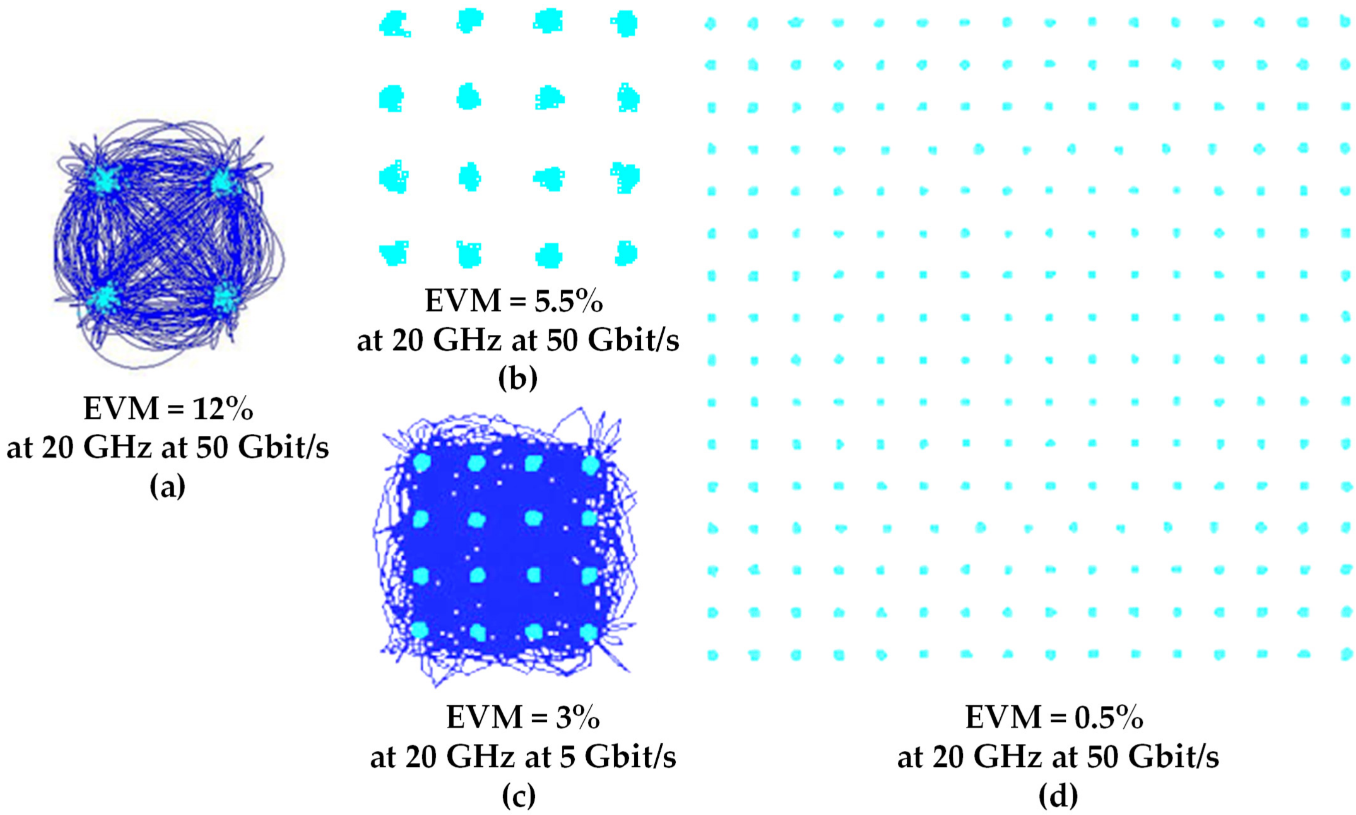

Figure 14. Constellation diagrams of the 4-QAM (**a**), 16-QAM (**b**,**c**), and 256-QAM (**d**) "AND" signals at the outbound port of the applied SOA-MZI.

6. Conclusions

For the sake of efficient performance and flexibility, logic "AND" gates are envisaged to be advantageous in all-optical application networks. In the above article, we advance a new concept for the three-input logic "AND" gate dependent on the SOA-MZI differential modulation mode. The XPM and XGM effects are observed using three OPS signals with a 2 ps pulse launched into the SOA-MZI. In addition, the gain measurements and ER for all logic "AND" gates are evaluated. The simulated ER of 56 and 50 dB are obtained at the SOA-MZI output at the harmonic frequency of 20 and 40 GHz, which is lower than the real ER by 2 dB, and the "AND" signal is obtained for the first time at 200 GHz in the simulation study. Furthermore, the gain is also lower for the experimental case and the whole “AND” system performance is unparalleled when the experimental results confirm the simulated results. As a result, the efficiency of the “AND” outcome is enhanced contingent on the SOA-MZI differential amendment approach with 2 ps optical pulse sources. In addition, the performance of this optical system is also evaluated through the EVM values at different bit rates where the maximum bit rates attained with 16-QAM and 256-QAM “AND” signals reach 100 and 200 Gbit/s, respectively. Additional logic gate principles including “NAND”, “OR”, and “NOR” will be of significance to achieve depending on the SOA-MZI differential modulation architecture.

Author Contributions: H.T. performed the principle, experiments, simulations, and prepared the manuscript; A.M. reviewed the manuscript. All authors have read and agreed to the published version of the manuscript.

Funding: This research received no external funding.

Data Availability Statement: Data underlying the results presented in this paper are not publicly available at this time but may be obtained from the authors upon reasonable request.

Conflicts of Interest: The authors declare no conflict of interest.

References

1. Kim, S.H.; Kim, J.H.; Yu, B.G.; Byun, Y.T.; Jeon, Y.M.; Lee, S.; Woo, D.H. All-optical NAND gate using cross-gain modulation in semiconductor optical amplifiers. *Electron. Lett.* **2005**, *41*, 1027–1028. [CrossRef]
2. Zhang, X.; Wang, Y.; Sun, J.; Liu, D.; Huang, D. All-optical AND gate at 10 Gbit/s based on cascaded single-port-couple SOAs. *Opt. Express* **2004**, *12*, 361–366. [CrossRef] [PubMed]
3. Kim, J.-Y.; Kang, J.-M.; Kim, T.-Y.; Han, S.-K. All-Optical Multiple Logic Gates With XOR, NOR, OR, and NAND Functions Using Parallel SOA-MZI Structures: Theory and Experiment. *J. Lightwave Technol.* **2006**, *24*, 3392.
4. Dong, J.; Zhang, X.; Xu, J.; Huang, D. 40 Gb/s all-optical logic NOR and OR gates using a semiconductor optical amplifier: Experimental demonstration and theoretical analysis. *Opt. Commun.* **2008**, *281*, 1710–1715. [CrossRef]
5. Li, Z.; Li, G. Ultrahigh-speed reconfigurable logic gates based on four-wave mixing in a semiconductor optical amplifier. *IEEE Photonics Technol. Lett.* **2006**, *18*, 1341–1343.
6. Sun, H.; Wang, Q.; Dong, H.; Dutta, N.K. XOR performance of a quantum dot semiconductor optical amplifier based Mach-Zehnder interferometer. *Opt. Express* **2005**, *13*, 1892–1899. [CrossRef]
7. Stubkjaer, K.E. Semiconductor optical amplifier-based all optical gates for high-speed optical processing. *IEEE J. Sel. Top. Quantum Electron.* **2000**, *6*, 1428–1435. [CrossRef]
8. Soto, H.; Topomondzo, J.D.; Erasme, D.; Castro, M. All-optical NOR gates with two and three input logic signals based on cross-polarization modulation in a semiconductor optical amplifier. *Opt. Commun.* **2003**, *218*, 243–247. [CrossRef]
9. Bintjas, C.; Kalyvas, M.; Theophilopoulos, G.; Stathopoulos, T.; Avramopoulos, H.; Occhi, L.; Schares, L.; Guekos, G.; Hansmann, S.; Dall'Ara, R. 20 Gb/s All-optical XOR operation with UNI Gate. *IEEE Photonics Technol. Lett.* **2000**, *12*, 824–836. [CrossRef]
10. Awad, E.S.; Cho, P.; Goldhar, J. High-Speed All-Optical AND Gate Using Nonlinear Transmission of Electro absorption Modulator. *IEEE Photonics Technol. Lett.* **2001**, *13*, 472–474. [CrossRef]
11. Agrawal, M.; Trivedi, K. All Optical Frequency encoded AND Gate using SOAs and Intensity Switch. In Proceedings of the 2012 Symposium on Photonics and Optoelectronics, Shanghai, China, 21–23 May 2012; ISBN 978-1-4577-0911-1112.
12. Li, Z.; Liu, Y.; Zhang, S.; Ju, H.; de Waardt, H.; Khoe, G.D.; Lenstra, D. All-optical logic gates based on an SOA and an optical filter. In Proceedings of the ECOC'05, Glasgow, UK, 25–29 September 2005.
13. Houbavlis, T.; Zoiros, K.E.; Kanellos, G.; Tsekrekos, C. Performance analysis of ultrafast all-optical Boolean XOR gate using semiconductor optical amplifier-based Mach–Zehnder Interferometer. *Opt. Commun.* **2004**, *232*, 179–199. [CrossRef]
14. Kim, J.H.; Jhon, Y.M.; Byun, Y.T.; Lee, S.; Woo, D.H.; Kim, S.H. All-optical XOR gate using a semiconductor optical amplifiers without additional beam. *IEEE Photonics Technol. Lett.* **2002**, *14*, 1436–1438.
15. Kim, S.H.; Kim, J.H.; Kim, G.; Byun, Y.T.; Woo, D.H. Implementation of all-optical logic AND using XGM based on semiconductor optical amplifier. In Proceedings of the COINNGNCON' 2006, Jeju, Republic of Korea, 9–13 July 2006; pp. 247–249.
16. Nesset, D.; Tathlam, M.C.; Cotter, D. All-Optical AND Gate Operating on 10 Gbit/s Signals at the Same Wavelength Using Four-Wave Mixing in a Semiconductor Laser Amplifier. *Electron. Lett.* **1995**, *31*, 896–897. [CrossRef]
17. Soto, H.; Díaz, C.A.; Topomondzo, J.; Erasme, D.; Schares, L.; Guekos, G. All-Optical AND Gate Implementation Using Cross-Polarization Modulation in a Semiconductor Optical Amplifier. *IEEE Photonics Technol. Lett.* **2002**, *14*, 498–500. [CrossRef]
18. Kumar, S.; Willner, A.E. Simultaneous four-wave mixing and cross-gain modulation for implementing an all-optical XNOR logic gate using a single SOA. *Opt. Express* **2006**, *14*, 5092–5097. [CrossRef]
19. Wang, Q.; Zhu, G.; Chen, H.; Jaques, J.; Leuthold, J.; Piccirilli, A.B.; Dutta, N.K. Study of All-Optical XOR using Mach-Zehnder Interferometer and Differential Scheme. *IEEE J. Quantum Electron.* **2004**, *40*, 703–710. [CrossRef]

20. Berrettini, G.; Simi, A.; Malacarne, A.; Bogoni, A.; Poti, L. Ultrafast integrable and reconfigurable XNOR, AND, NOR, and NOT photonic logic gate. *IEEE Photonics Technol. Lett.* **2006**, *18*, 917–919. [CrossRef]
21. Kotb, A. AND gate based on two-photon absorption in semiconductor optical amplifer. *Optoelectron. Lett.* **2013**, *9*, 181–184. [CrossRef]
22. Chen, X.; Huo, L.; Zhao, Z.; Zhuang, L.; Lou, C. Study on 100-Gb/s reconfigurable all-optical logic gates using a single semiconductor optical amplifer. *Opt. Express.* **2016**, *24*, 30245–30253. [CrossRef]
23. Kim, J.H.; Kim, B.C.; Byun, Y.T.; Jeon, Y.M.; Lee, S.; Woo, D.H. All-optical AND gate using cross-gain modulation in semiconductor optical amplifers. *Jpn. J. Appl. Phys.* **2004**, *43*, 608–610. [CrossRef]
24. Kang, B.-K.; Kim, J.H.; Byun, Y.T.; Lee, S.; Jhon, Y.M.; Woo, D.H.; Yang, J.S.; Kim, S.H.; Park, Y.H.; Yu, B.G. All-optical AND gate using probe and pump signals as the multiple binary points in cross phase modulation. *Jpn. J. Appl. Phys.* **2002**, *41*, L568–L570. [CrossRef]
25. Dimitriadou, E.; Zoiros, K.E. On the design of reconfigurable ultrafast all-optical NOR and NAND gates using a single quantum-dot semiconductor optical amplifier-based Mach-Zehnder interferometer. *J. Opt.* **2012**, *14*, 105401. [CrossRef]
26. Kotb, A.; Mohamed, Y. Phase-Shift Keying Modulated Data Signal Using SOA-MZI-Based All-Optical Logic AND Gate at 80 Gb/s. *Int. J. Opt.* **2018**, *2018*, 1–8. [CrossRef]
27. Mikkelsen, B.; Durhuus, T.; Joergensen, C. 10 Gbit/s wavelength converter realized by monolithic integration of semiconductor optical amplifiers and Michelson interferometer. In Proceedings of the 20th European Conference on Optical Communication (ECOC '94), Firenze, Italy, 25–29 September 1994; pp. 67–70.
28. Zoiros, K.E.; Houbavlis, T.; Kanellos, G.T. Theoretical analysis and performance investigation of ultrafast all-optical Boolean XOR gate with semiconductor optical amplifier-assisted Sagnac interferometer. *Opt. Commun.* **2006**, *258*, 114–134. [CrossRef]
29. Senior, J.M. *Optical Fiber Communication*, 3rd ed.; Pearson Education: Harlow, UK, 2010.
30. Runge, P.; Bunge, C.A.; Petermann, K. All-Optical Wavelength Conversion with Extinction Ratio Improvement of 100 Gb/s RZ-Signals in Ultralong Bulk Semiconductor Optical Amplifiers. *IEEE J. Quantum Electron.* **2010**, *46*, 937–944. [CrossRef]
31. Leuthold, J.; Marom, D.M.; Cabot, S.; Jaques, J.J.; Ryf, R.; Giles, C.R. All-optical wavelength conversion using a pulse reformatting optical filter. *J. Lightwave Technol.* **2004**, *22*, 186–192. [CrossRef]
32. Liu, Y.; Tangdiongga, E.; Li, Z.; De Waardt, H.; Koonen, A.M.; Khoe, G.D.; Dorren, H.J.; Shu, X.; Bennion, I. Error-free 320 Fb/s SOA-Based Wavelength Conversion Using Optical Filtering. In Proceedings of the 2006 Optical Fiber Communication Conference and the National Fiber Optic Engineers Conference, Anaheim, CA, USA, 5–10 March 2006.
33. Contestabile, G.; Presi, M.; Ciaramella, E. Multiple wavelength conversion for WDM multicasting is a SOA. *IEEE Photonics Technol. Lett.* **2004**, *16*, 1775–1777. [CrossRef]
34. Dong, H.; Sun, H.; Wang, Q. 80 Gb/s All-optical logic AND operation using Mach-Zehnder interferometer with differential scheme. *Opt. Commun.* **2006**, *265*, 79–83. [CrossRef]
35. Kang, B.-K.; Kim, J.H.; Park, Y.H.; Lee, S.; Jhon, Y.M.; Woo, D.H.; Kim, S.H.; Park, S.-H. All-optical logic AND in a SOA-based Mach-Zehnder all-optical wavelength converter. In Proceedings of the 13th Laser and Electro-Optics Society, Rio Grande (Puerto Rico), TX, USA, 13–16 November 2000; Volume 1, pp. 117–118.
36. Singh, P.; Tripathi, D.K.; Jaiswal, S.; Dixit, H.K. Design and analysis of all-optical AND, XOR and OR gates based on SOA–MZI configuration. *Opt. Laser Technol.* **2015**, *66*, 35–44.
37. VPI Transmission Maker/VPI Component Maker, User's Manual, Photonic Modules Reference Manuals. VPI Photonics Official Website. Available online: http://www.vpiphotonics.com (accessed on 14 June 2022).
38. Termos, H. Study of Up and Down Conversion Technique by All Optical Sampling Based on a SOA-MZI. Ph.D. Thesis, Université de Bretagne Occidentale, Brest, France, February 2017.
39. Termos, H.; Rampone, T.; Sharaiha; Hamie, A.; Alaeddine, A. All-Optical Radiofrequency Sampling Mixer Based on a Semiconductor Optical Amplifier Mach–Zehnder Interferometer Using a Standard and a Differential Configuration. *J. Lightwave Technol.* **2016**, *34*, 4688–4695. [CrossRef]
40. Termos, H.; Rampone, T.; Sharaiha; Hamie, A.; Alaeddine, A. Up and down frequency conversion of a QPSK signal by an all-optical radiofrequency sampling mixer based on a semiconductor optical amplifier Mach-Zehnder interferometer. In Proceedings of the 2015 International Topical Meeting on Microwave Photonics (MWP), Paphos, Cyprus, 26–29 October 2015; pp. 1–4.
41. Termos, H.; Rampone, T.; Sharaiha; Hamie, A.; Alaeddine, A. OFDM signal up and down frequency conversions by a sampling method using a SOA-MZI. In Proceedings of the 2017 29th International Conference on Microelectronics (ICM), Beirut, Lebanon, 10–13 December 2017; pp. 1–5.
42. Termos, H.; Rampone, T.; Sharaiha, A. Sampling rate influence in up and down mixing of QPSK and OFDM signals using an SOA-MZI in a differential configuration. *Electron. Lett.* **2018**, *54*, 990–991. [CrossRef]
43. Fernandez, A.; Chao, L.; Chi, J.W.D. All-optical clock recovery and pulse reshaping using semiconductor optical amplifier and dispersion compensating fiber in a ring cavity. *IEEE Photonics Technol. Lett.* **2008**, *20*, 1148–1150. [CrossRef]
44. Valaddmir, S. *Test Data and Operation Manual of Ultrafast Optical Clock*; Pritel, Inc.: Naperville, IL, USA, 2014.
45. Termos, H.; Mansour, A. OFDM signal down frequency conversion based on a SOA-MZI sampling mixer using differential modulation and switching architectures. *Optik* **2021**, *245*, 167761. [CrossRef]

46. Spyropoulou, M.; Pleros, N.; Miliou, A. SOA-MZI-based nonlinear optical signal processing: A frequency domain transfer function for wavelength conversion, clock recovery, and packet envelope detection. *IEEE J. Quantum Electron.* **2011**, *47*, 40–49. [CrossRef]
47. Mathlouthi, W.; Vacondio, F.; Lemieux, P.; Rusch, L.A. SOA gain recovery wavelength dependence: Simulation and measurement using a single-color pump-probe technique. *Opt. Express* **2008**, *16*, 20656. [CrossRef] [PubMed]
48. Ginovart, F.; Simon, J.C. Wavelength dependence of gain recovery time in a semiconductor optical amplifier based wavelength shifter. In Proceedings of the IEEE CLEO, Munich, Germany, 22–27 June 2003; p. 181.
49. Termos, H.; Mansour, A.; Nasser, A. Simultaneous up- and down-frequency mixing based on a cascaded SOA-MZIs link. *Appl. Opt.* **2021**, *60*, 8336. [CrossRef]
50. Schmogrow, R.; Nebendahl, B.; Winter, M.; Josten, A.; Hillerkuss, D.; Koenig, S.; Meyer, J.; Dreschmann, M.; Huebner, K.; Koos, C.; et al. Error vector magnitude as a performance measure for advanced modulation formats. *IEEE Photonics Technol. Lett.* **2012**, *24*, 61–63. [CrossRef]
51. Mestre, M.A.; Mardoyan, H.; Caillaud, C.; Rios-Muller; Renaudier, J.; Jenneve, P.; Blache, F.; Pommereau, F.; Decobert, J.; Jorge, F.; et al. Compact InP-based DFB-EAM enabling PAM-4 112 Gb/s transmission over 2 km. *J. Lightwave Technol.* **2016**, *34*, 1572–1578. [CrossRef]
52. Cai, Y.; Ramanujam, N.; Morris, J.M.; Adali, T.; Lenner, G.; Puc, A.B.; Pilipetskii, A. Performance limit of forward error correction codes in optical fiber communications. In Proceedings of the Optical Fiber Communication (OFC) Conference and Exhibit, Anaheim, CA, USA, 17–22 March 2001; Volume 2, p. TuF2-1.
53. Nguyen, D.-N.; Bohata, J.; Spacil, J.; Dousek, D.; Komanec, M.; Zvanovec, S.; Ghassemlooy, Z.; Ortega, B. M-QAM transmission over hybrid microwave photonic links at the K-band. *Opt. Express* **2019**, *27*, 33745–33756. [CrossRef]
54. Argyris, N.; Kanta, K.; Iliadis, N.; Giannoulis, G.; Apostolopoulos, D.; Avramopoulos, H.; Papaioannou, S.; Vagionas, C.; Kalfas, G.; Pleros, N. DSP enabled Fiber-Wireless IFoF/mmWave link for 5G Analog Mobile Fronthaul. In *2018 IEEE 5G World Forum (5GWF)*; IEEE: Silicon Valley, CA, USA, 2018; pp. 482–487.
55. 3GPP, TS 38.104 V15.0.0, Table 9.6.2.3-1, December 2017. Available online: https://www.etsi.org/deliver/etsi_ts/138100_138199/138104/15.02.00_60/ts_138104v150200p.pdf (accessed on 15 February 2023).